Structure and Properties of Y_2O_3-Doped Al_2O_3-MWCNT Nanocomposites Prepared by Pressureless Sintering and Hot-Pressing

Iftikhar Ahmad & Mushtaq Ahmad Dar

Journal of Materials Engineering and Performance

ISSN 1059-9495
Volume 23
Number 6

J. of Materi Eng and Perform (2014)
23:2110-2119
DOI 10.1007/s11665-014-0975-y

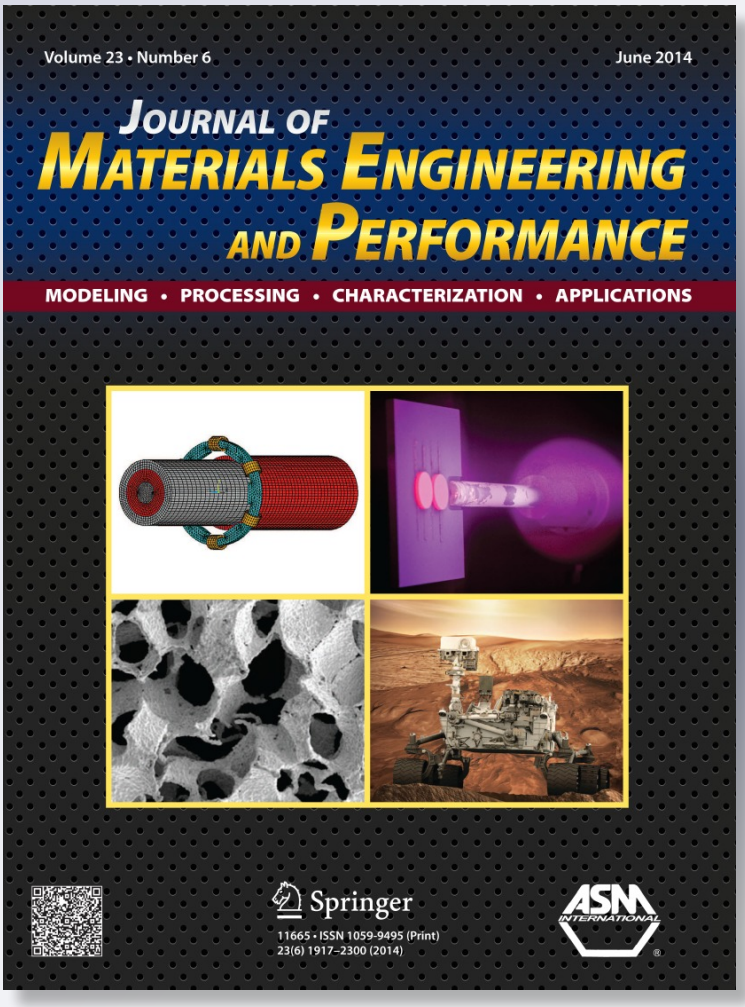

Springer

JMEPEG (2014) 23:2110–2119
DOI: 10.1007/s11665-014-0975-y

1059-9495/$19.00

Structure and Properties of Y_2O_3-Doped Al_2O_3-MWCNT Nanocomposites Prepared by Pressureless Sintering and Hot-Pressing

Iftikhar Ahmad and Mushtaq Ahmad Dar

(Submitted January 23, 2014; in revised form March 16, 2014; published online April 11, 2014)

This study describes the combined effects of multi-walled carbon nanotubes (CNTs) additions and Y_2O_3 doping on the microstructures and mechanical properties of Al_2O_3-CNT nanocomposites fabricated by pressureless and hot-press sintering processes. A uniform dispersion of CNTs within the Al_2O_3 matrix was successfully attained via a combined approach using surfactant, sonication, and adequate period of incubation. Small amounts (1 wt.%) of Y_2O_3, as dopants, significantly affected the densification and properties of pressureless sintered monolithic Al_2O_3 and its nanocomposites at low CNT concentrations (< 1 wt.%); however, they hardly showed any improvement at higher CNT contents. As opposed to the pressureless sintering, pressures applied during high temperature sintering in combination with the Y_2O_3 doping contributed in generating a homogenous microstructure and improved the densities (7 and 15%) and microhardness (11 and 12%) of Al_2O_3 reinforced with higher CNT contents (2 and 5 wt.%), respectively. Adding on, hot-pressed Y_2O_3-doped Al_2O_3 reinforced with 2 and 5 wt.% CNTs showed higher hardness (19 and 70%), flexural strength (10 and 5%), and fracture toughness (26 and 11%), respectively, compared to similar but CNT-free samples. These results showed that pressure-assisted sintering and Y_2O_3 are promising for the fabrication of CNT-reinforced Al_2O_3 nanocomposites, especially at higher CNT concentrations.

Keywords carbon nanotube (CNT), nanocomposite, microstructure, sintering, Y_2O_3

1. Introduction

CNTs are very attractive nanomaterial. Both structures of CNTs, single and multi-walled, have excellent mechanical properties, with modulus of elasticity around 1TPa, high elasticity nearly 40%, and promising tensile strength of 500 GPa (Ref 1). Exceptional electrical, physical, and mechanical characteristics of CNTs have inspired us to utilize theses nanomaterials for diverse multi-functional applications (Ref 2). Nanocomposite materials are an important topic in materials technology, especially the concept to use the CNTs, as a reinforcing agent in hard ceramics. Among ceramics, Al_2O_3 is one of the most widely used material having high hardness, good oxidation resistance, and chemical stability; however, its fracture toughness makes it inadequate for certain advanced applications (Ref 3). In this context, flexible and strong CNTs are thought to be a promising material to curtail the brittleness of Al_2O_3 ceramics. Contemporary research on the CNTs-reinforced Al_2O_3 has shown some improvements in fracture toughness and other mechanical properties (Ref 4-8). CNTs in Al_2O_3 ceramics hampered the densification process, refined the matrix by grain pinning, increased the fracture toughness by crack bridging/crack deflection, improved the wear resistance by sliding/rolling, and enhanced the electrical/thermal properties (Ref 5-10). Despite using distinct dispersion techniques (hetro-coagulation, mechanical mixing, ball milling, and sol-gel), obtained thorough dispersion of CNTs is unfortunately still the biggest challenge in CNTs-reinforced ceramics nanocomposite manufacturing (Ref 6-12). Strong Van der Waals interactions and high aspect ratio are mainly responsible for the agglomeration tendency of the nanotubes (Ref 4-12). Presumably, the CNTs agglomerations and weak interfaces between CNTs and the matrix may be the possible cause of inferior quality of the nanocomposites. Thus, achieving a homogenous dispersion of CNTs in ceramic oxides and with strong bonding between the nanotubes and matrix is a challenging task. Furthermore, CNTs contributed to matrix grains refinement but increased the sintering temperature, thus becoming a new hurdle to achieve near theoretical density, as described in some recent studies (Ref 8-12). To attain higher densities in Al_2O_3-CNT nanocomposites, most attempted spark plasma sintering (SPS) and hot-pressing (HP) sintering processes, but very few practiced pressure-free sintering (Ref 8-10, 13).

Improving the structure and properties of pure Al_2O_3 and Al_2O_3-based matrices with metal oxide dopants such as MgO, Ce_2O_3, Li_2O, and Y_2O_3 has been well-known practice (Ref 14-19). For example, the addition of > 1000 ppm MgO significantly increase the sintered density of pressureless sintered Al_2O_3-5 vol% SiC nanocomposites (Ref 21). Small amounts of MgO (300 ppm) reduced the effective sintering temperature to nearly 1600 °C and restricted the grain growth of Al_2O_3 matrix (Ref 20, 21). Similarly, the additions of yttrium oxide,

Iftikhar Ahmad and **Mushtaq Ahmad Dar,** Center of Excellence for Research in Engineering Materials, Advanced Manufacturing Institute, King Saud University, P. O. Box. 800, Riyadh 11421, Kingdom of Saudi Arabia. Contact e-mail: ifahmad@ksu.edu.sa.

Y_2O_3 (<1000 ppm), increased the monolithic Al_2O_3 and ZrO_2-reinforced Al_2O_3 to higher densities (99%), with fine-grained microstructure and higher mechanical properties (Ref 17, 20-24). Despite these successes, the potential benefits of Y_2O_3 have not yet been attained in CNT-reinforced Al_2O_3 nanocomposites; therefore, interesting results are anticipated.

In this context, we report the synthesis, structural characterization, and the mechanical performance of the Y_2O_3-doped Al_2O_3-CNTs nanocomposites fabricated by pressureless and pressure-assisted (hot-press) sintering processes. The main aims of this study are (i) to explore a rather convenient colloidal chemistry-based CNTs dispersion method for obtaining homogenous distribution of CNTs into Al_2O_3 matrix, (ii) to prepare highly dense CNTs-reinforced Al_2O_3 nanocomposites with the assistance of Y_2O_3 through pressureless and hot-press sintering routes, and (iii) to identify the combined role of CNTs (as reinforcing agent) and Y_2O_3 (as dopant) on the hardness Vickers (HV), fracture toughness (K_{IC}), flexural strength (σ_y), and modulus of elasticity (E) of the Al_2O_3 ceramic. Moreover, the role of Y_2O_3 in microstructural tuning of the Al_2O_3-CNTs nanocomposites is also presented.

2. Experimental Procedure

2.1 Materials and Sample Preparation

Multi-walled CNTs having an outer diameter of ~40 nm (Tsinghua University, Beijing, China), as shown in Fig. 1a, were chemically modified with H_2SO_4-HNO_3 solution and then dispersed into an aqueous solution containing a small quantity (1 wt.% of CNTs) of sodium dodecyl sulfate (SDS, Sigma-Aldrich, UK), a surfactant, with the help of sonication for 30 min using an ultrasonic probe (Sonic Processor D-100-20, Sonic system, UK). The CNT slurry was incubated for 2 weeks, in order to thoroughly adsorb the surfactant onto the CNT surfaces. Nanopowder of Al_2O_3 ceramics, shown in Fig. 1b, with mean size of <50 nm (Sigma Aldrich, UK) was then added and sonicated again for 60 min to get thorough mixing. After drying at 120 °C, the mixture was then milled and compacted at a pressure of 800 MPa into 12-mm-diameter tablets using uniaxial press (Moor Hydraulic Press, UK) and subsequently sintered at 1600 °C for 60 min under Ar in a tube furnace (Elite, UK). Unreinforced Al_2O_3 tablets, without CNTs, were also fabricated using the same method. An appropriate quality of Y_2O_3 of mean diameter 25-30 nm (Sigma Aldrich, UK), was incorporated in all samples in order to promote sintering. Nanocomposites were also hot-pressed (University of Mining and Technology, China) under a pressure of 30 MPa at 1600 °C for 60 min under vacuum.

2.2 Structural Characterization and Mechanical Testing

Structural features of fractured samples were assessed by scanning electron microscopy (SEM, PHILIPS XL30, operated at 20 kV), and prior to SEM observation, all samples were coated with thin layer of gold. Transmission electron microscopy (FEG-TEM, JEOL 2100F) was used to characterize the nanocomposite and its constituents. For TEM analysis, nanocomposite samples were initially crushed into small pieces and then chemically etched using NaOH for 2 weeks followed by a thorough rinsing with distilled water for complete removal of NaOH. The clean recovered samples were then dispersed in acetone and shifted

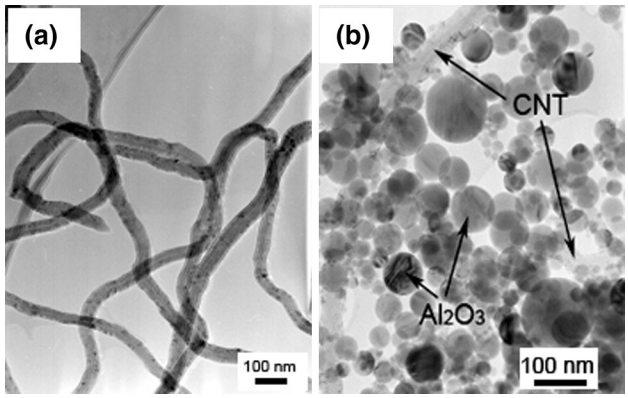

Fig. 1 (a) Pristine CNTs and (b) mixture of CNTs and Al_2O_3 nanoparticles

onto a holey carbon film, supported on a copper grid, for further TEM examination. A Siemens D500 x-ray diffractometer with CuKα radiation was used at scan rate of 0.025°/s to identify the crystalline phases present in the sintered samples, with the assistance of computer software (DIFFRACplus by Bruker Advanced x-ray Solutions). Densities of the sintered samples were measured by Archimedes method in distilled water, and the relative density was calculated by dividing the apparent density by theoretical density. Theoretical densities for Al_2O_3, Y_2O_3, and CNTs of 3.9, 5.0, and 1.8 g/cm^3, respectively, were used for relative densities calculations in this work (Ref 7, 25). Thermal etching of finely polished sintered samples was performed in a tube furnace under an Ar atmosphere at 1400 °C for 15 min to determine the grain size and grain boundary studies.

For microhardness evaluation, the sintered nanocomposite samples were fractured and cold mounted. During cold mounting, the samples were vacuum infiltrated using epoxy resin. After mounting, the samples were first ground on diamond pads of 120 and 220 grits and then polished to 6 and 1 μm by using DP-Suspension on polishing cloths. Microhardness testing was carried out at 9.8 N loads for 15 s (M-400 hardness tester, LECO, Japan). The diagonal length of the diamond indent was measured using the attached microscope, converted to Vickers hardness number (HV), and further converted to GPa.

Sintered samples were also cut into rectangular bars of 25 ± 1.5 mm (length) $\times 2 \pm 0.15$ mm (breadth) $\times 2.5 \pm 0.20$ mm (height), three-point bending performed was performed using 20 mm bending span and 0.50 mm/min of testing speed, and the flexural (σf) strength was calculated by employing Eq 1, where F is the load at the fracture point, L is the span length, b is the sample breath, and d is the sample thickness (Ref 9).

$$\sigma_f = \frac{3FL}{2bd^2}. \quad \text{(Eq 1)}$$

The modulus of elasticity (E) of all samples was calculated by standard pulse-echo technique. Equation 2 was used to estimate the values of the Young's modulus (E), where ρ is the bulk density of the sample, Vc is the compression velocity and Vs the shear velocity (Ref 26).

$$E = \frac{V_s^2 \rho \left(3V_c^2 - 4V_s^2\right)}{V_c^2 - V_s^2}. \quad \text{(Eq 2)}$$

The direct crack method (ICM) was used to estimate the fracture toughness (K_{IC}) of sintered samples. The length of

cracks generated during indentation was carefully measured from the centre by using scanning electron microscopy, (Philips/FEI XL30 FEG-ESEM), in combination with computer software ImageJ (Image Processing and Analysis in Java).

$$K_{IC} = 0.016\left(\frac{E}{H}\right)^{1/2}\left(\frac{P}{c^{3/2}}\right). \quad \text{(Eq 3)}$$

The fracture toughness was calculated by above mentioned Eq 3, where E is the modulus of elasticity, H is the hardness, and c is the radial crack length generated by Vickers's indentation (Ref 27).

3. Results and Discussion

3.1 Homogenous Dispersions of CNTs

Achieving a homogenous dispersion of CNTs within the matrix is a foremost challenge to manufacture CNTs-reinforced nanocomposites with superior mechanical properties. CNTs have the tendency to agglomerate, forming clusters and acting as impurities in nanocomposites, and consequently obstruct the interconnection with the matrix (Ref 6). In this viewpoint, the homogenous dispersion of CNTs in the matrix may have vital impact on the mechanical properties of the nanocomposites. The dispersion behavior of CNTs in aqueous solution was assessed in three stages as displayed in Fig. 2a. CNTs tended to settle whenever trying to obtain a suspension due to their hydrophobic nature, poor wetting characteristics, and difference in density, as shown in Fig. 2a(i). After the addition of a small quantity of surfactant (SDS), a partial dispersion of CNTs was achieved as demonstrated in Fig. 2a(ii), because the addition of SDS improved the dispersion capability of water by decreasing its surface tension. It is believed that proper adsorption of the surfactant on the CNT's surface and the uniform suspension of CNT's in water was achieved after 2 weeks of incubation time, as exhibited in Fig. 2a(iii). Molecular modeling has shown the aliphatic dodecyl groups to partially wrap around the CNT (see Fig. 2b and c), while ionized sulfate group sticks out in the water to provide hydrophilicity. The negative charges of the ionized sulfate group cause repulsion among the CNT's (Ref 28). The dispersion of CNTs in the Al_2O_3 matrix was also assessed by SEM examination of the fractured nanocomposite samples. Homogenous dispersion was achieved after an incubation period of 2 weeks after SDS was added to the CNT solution before mixing with the ceramic powders, as shown in Fig. 3(c) and (d). Nanocomposites manufactured without the addition of SDS exhibited severe agglomeration as demonstrated in Fig. 3a, in which huge agglomerates of CNTs are clearly visible. Individually well-dispersed CNTs, having good connection with the ceramic grains, have been revealed at higher magnification in Fig. 3d.

3.2 Densification and Physical Properties

To achieve high densities for Al_2O_3-based nanocomposites, the selection of Y_2O_3 contents is critical. For this reason, various amounts of Y_2O_3 (0.5, 1.0 and 1.5 wt.%) were doped into monolithic Al_2O_3 and Al_2O_3-1 wt.% CNT, in order to optimize the Y_2O_3 contents for achieving high densities. Figure 4b shows that a small addition of Y_2O_3 enhanced the density of monolithic Al_2O_3; however, further addition did not

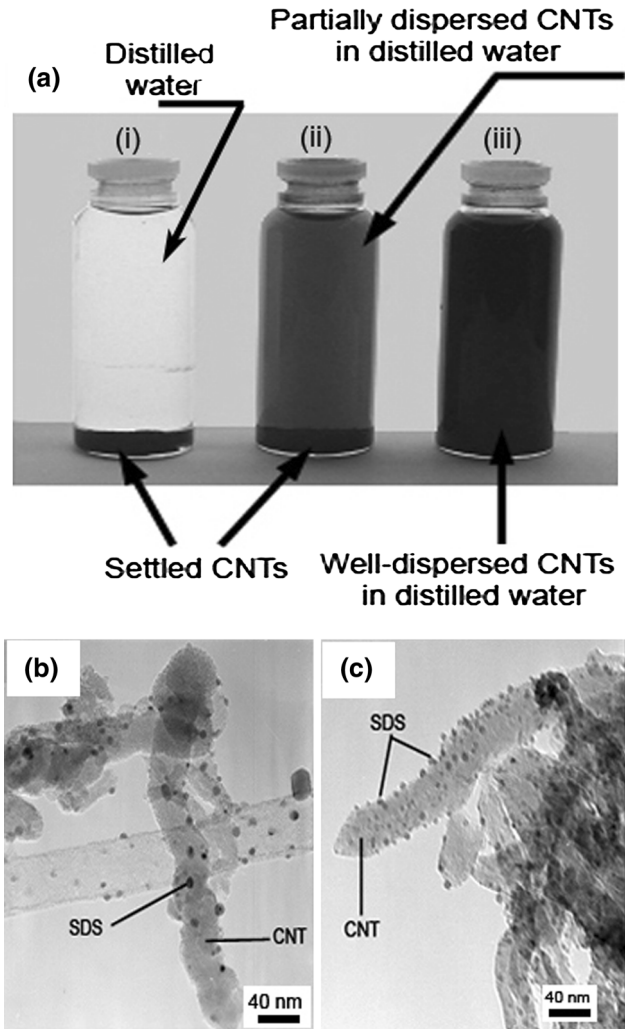

Fig. 2 (a) CNTs in an aqueous solution (i) agglomerated CNTs, (ii) partially suspended CNTs, (ii) homogenously suspended CNTs, TEM images of (b) SDS around CNTs and (c) SDS adsorption on CNTs after 2 weeks

display significant improvement. In contrast to this, addition of Y_2O_3 in Al_2O_3-1 wt.% CNT nanocomposites exhibited considerable increase in density and a maximum density was observed at 1 wt.% addition. After the optimal Y_2O_3 content (1 wt.%) was established, various amounts of CNTs (0, 0.5, 1, 2, and 5 wt.%) were then used to reinforce the Al_2O_3, to investigate the effects of CNT on the density, and the results are demonstrated in Fig. 4c, for pure and CNT-reinforced Al_2O_3. Gradual improvements of 5, 6, 8, 7, and 6% in densities for the addition of 0, 0.5, 1.0, 2.0, and 5.0 wt.% CNTs were observed with 1 wt.% Y_2O_3 content, respectively. XRD pattern revealed the typical peaks for α-Al_2O_3 (JCPDS card no. 01-078-2426), as shown in Fig. 5a(i). Due to the high crystalline features of the α-Al_2O_3 phase and low contents of CNT in the nanocomposites, no CNT peak (JCPDS card no. 01-075-1621) was identified. However, peaks of $Y_3Al_5O_{12}$, yttrium aluminium garnet (YAG) according to JCPDS card no. 01-072-1853, can be seen in Fig. 5a (iv).

These results corroborate that the addition of Y_2O_3 increased the sinterability of Al_2O_3-based nanocomposites (Ref 29). A slight increase in the density of Y_2O_3-doped

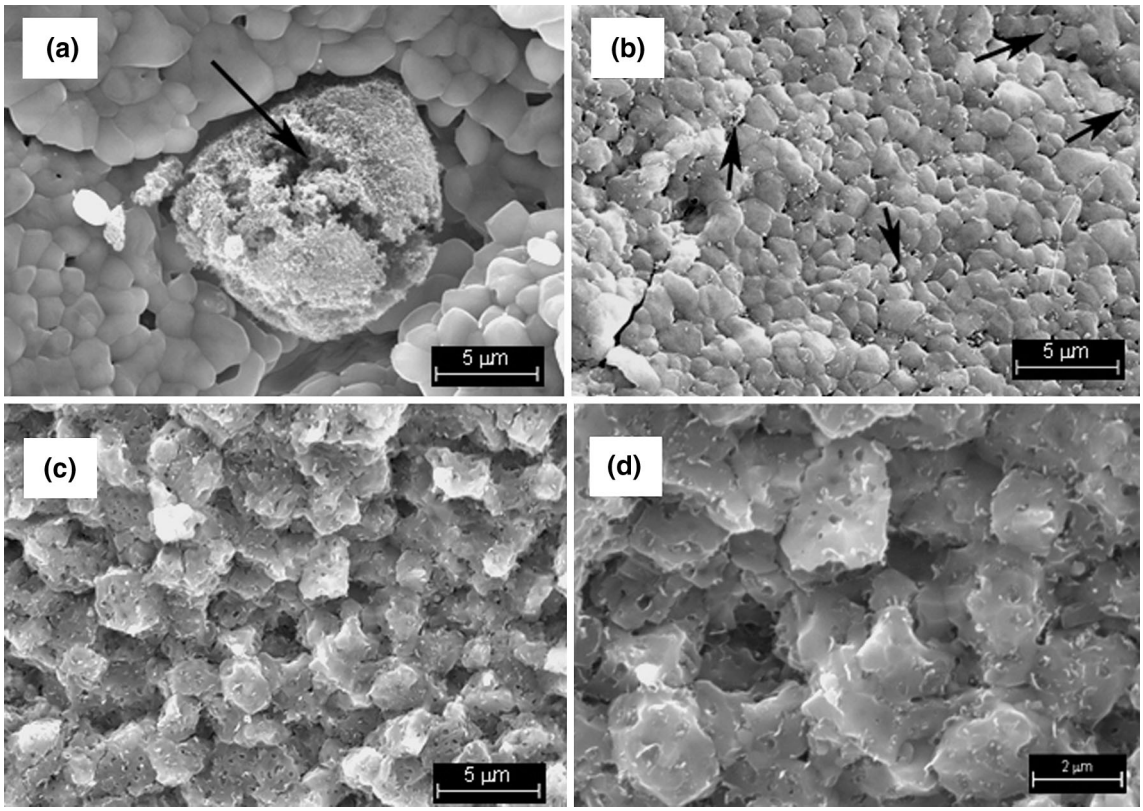

Fig. 3 SEM images of Al_2O_3-CNTs nanocomposites (a) agglomerated CNTs (black arrows), (b) partially dispersed CNTs and well-dispersed CNTs at (c) low and (d) high magnifications (white arrows)

Al_2O_3 and Al_2O_3-CNT nanocomposites can be associated with the formation of a new phase at the grain boundary and was identified as YAG, as confirmed in the XRD pattern in Fig. 5a, and further EDX analysis of thermally etched sample verifies the elemental constituents of YAG phase at the grain boundaries Al_2O_3 in Fig. 5b. Y_2O_3 generally inhibited the grain growth in pure Al_2O_3 through the blocking of grain boundary diffusion by segregated Y_2O_3 and the formation of YAG phase at the grain boundary. In this context, it is shown that the results agreed well with the previous works (Ref 30). Based on the presence of a new phase at the Al_2O_3 grain boundaries, as clearly evident in Fig. 5b, it may be suggested that a new phase is formed during the sintering of Al_2O_3 in the presence of Y_2O_3. YAG precipitates are thermodynamically formed from Y_2O_3-Al_2O_3 solid solution thorough phase-transformation process thus their existence and thorough distributions in the overall microstructure are rational, compared to the dispersions of CNTs in the Al_2O_3 matrix (Ref 31-33). Being a second phase, CNTs are accumulated at Al_2O_3 grain boundaries during the sintering process. Obviously, the CNT population at Al_2O_3 grain boundaries was increased at higher CNT additions (>2 wt.%). It is quite possible that large concentrations of CNT at the grain boundaries suppressed the formation of YAG at grain boundary and hindered the coalescence of Al_2O_3 grains, resulting in Al_2O_3-CNT nanocomposites with poor densification. In contrast to this, no such hurdle is present in case of unreinforced Al_2O_3. Therefore, increase in density by adding Y_2O_3 thus could be elucidated by the formation of YAG phase at the grain boundaries.

Hot-pressing involves the simultaneous application of pressure and heat to a powder system to achieve higher densities and better mechanical properties. Pressure-assisted sintering improved the density (7 and 15%) and hardness (11 and 12%) at CNTs loading (2 and 5 wt.%), respectively, of the CNT-reinforced Y_2O_3-doped Al_2O_3, as opposed to the pressureless sintered samples shown in Fig. 4d. During hot-pressing, the high density of Y_2O_3-doped Al_2O_3 is due to accelerated densification which can be attributed to an increased stress due to the externally applied pressure, which consolidates the grain to a higher density (Ref 34). The increase in density of Al_2O_3-CNT nanocomposites is, possibly, due to the combined effect of applied pressures and CNT because CNT reduces the grain size by pinning the grain boundaries and develops nanocomposites structure with fine grains. On the basis of microhardness results, it can be predicted that the pressure-assistance during the high temperature sintering process also increased the interaction between the CNT and matrix which is responsible for good cohesion between them by forming strong interface, as suggested earlier (Ref 35).

3.3 Microstructural Analysis

The results of adding Y_2O_3 on the grain size of pure and CNT-reinforced Al_2O_3 are graphically demonstrated in Fig. 6 and structurally shown in Fig. 7. Figure 7a shows the microstructure of the undoped sample. Mainly, Y_2O_3 affected the grain size in two ways. Firstly, Y_2O_3 addition promoted the abnormal grain growth, as shown in Fig. 7d. The resulting large grain size (10%) of monolithic Al_2O_3, due to Y_2O_3 additions, is in good agreement with previous work and is thought to be associated with the formation of small and large grains in a bimodal distribution, and the reason for the large mean grain

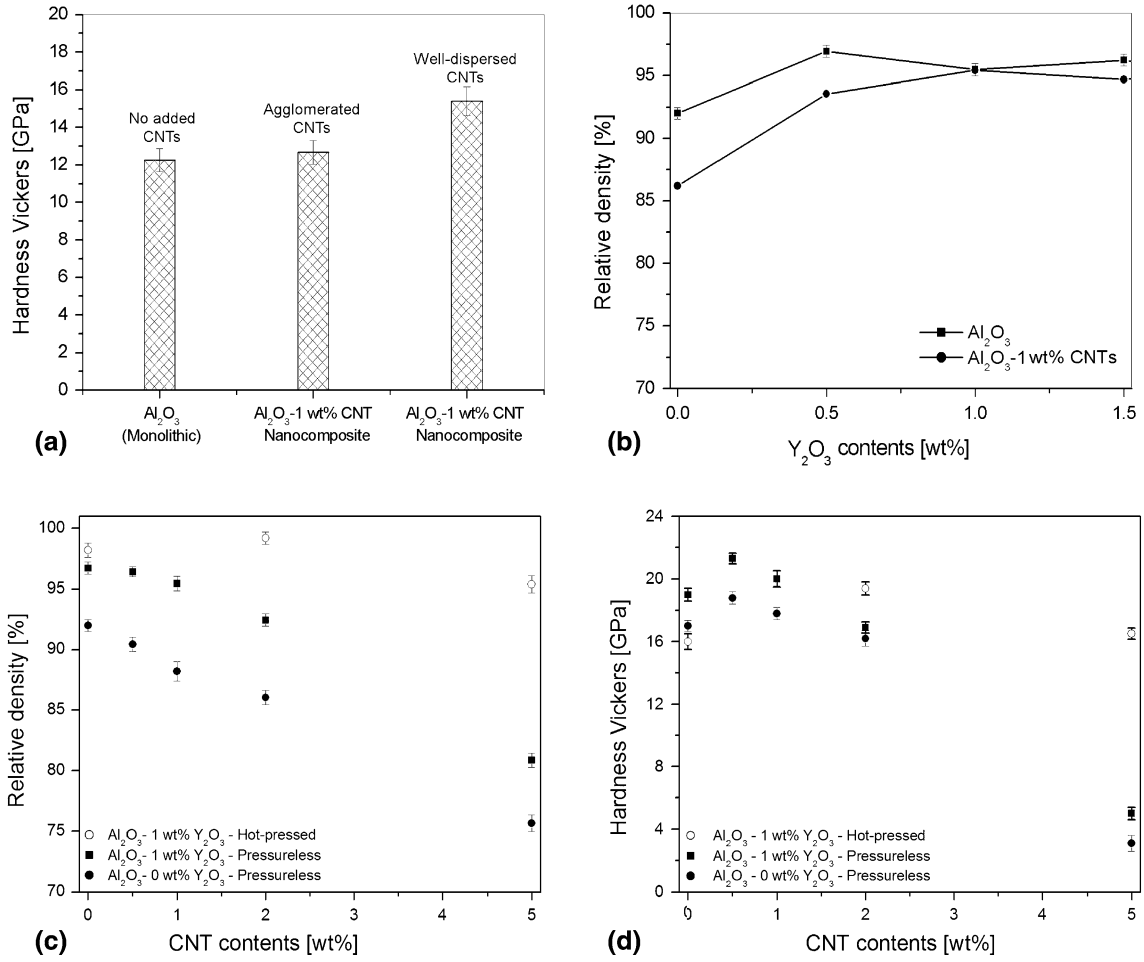

Fig. 4 Effects of (a) CNT dispersions on the hardness of the Al_2O_3-1 wt.% CNT nanocomposites fabricated by pressureless sintering, (b) Y_2O_3 contents on the density of monolithic Al_2O_3 and Al_2O_3-1 wt.% CNT nanocomposite and the CNT contents on (c) density and (d) hardness of 1 wt.% Y_2O_3-doped Al_2O_3

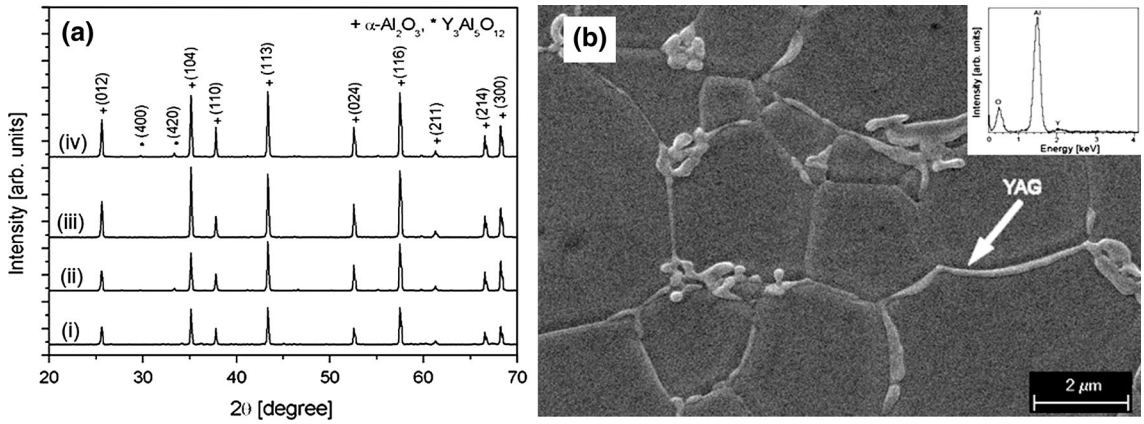

Fig. 5 (a) XRD patterns of (i) Monolithic Al_2O_3, (ii) Al_2O_3-1 wt.% Y_2O_3, (iii) Al_2O_3-2 wt.% CNT, (iv) Al_2O_3-1 wt.% Y_2O_3-2 wt.% CNT and (b) thermally etched image of Y_2O_3-doped Al_2O_3 clearly showing the presence of YAG at grain boundary and inset shows EDX analysis confirming YAG

size is due to having more abnormally large grains (Ref 34). Secondly, Y_2O_3 itself destabilized the grain growth by the formation of YAG. This phenomenon is evident from Fig. 7d, where abnormal grain growth due to Y_2O_3 additions is visible. Y_2O_3 additions in the Al_2O_3-CNT nanocomposites also encouraged the abnormal grain growth, but the pinning effects of CNT restricted the grain growth and limited the formation of abnormal grains, therefore, ultimately modified the grain

structure. An obvious difference lies in the 80% smaller grains of Al_2O_3-CNT nanocomposites when compared with the monolithic Al_2O_3, as presented in Fig. 7(e) and (f).

Hot-pressed samples revealed interesting microstructural features. Compared to pressure-free sintered, the hot-pressed Y_2O_3-doped Al_2O_3 exhibited 8% larger grains and in case of doped nanocomposites, 20 and 25% larger grain sizes for 2 and 5 wt.% CNT additions were also observed, as demonstrated in Fig. 6 and 7(d-i). The development of large grains during HP is believed to be associated with the drag forces on boundary motion, because applied pressures during sintering increased the densification rate, resulting in the reduction of drag forces during the sintering process which in turn generates large grain structures with homogenous size. Consequently, density and hardness increased (Ref 36). Hence, it is possible that the addition of Y_2O_3 had no significant effect on the grain refinement during HP but may have altered the sintering characteristics of Al_2O_3 in the nanocomposites. It was also noted that under Ar protection, it is very difficult to achieve 100% of the theoretical density with pressureless sintering of the nanocomposites due to decomposition of Al_2O_3 at high temperatures >1600 °C and resulting in O_2 losses from Al_2O_3 (Ref 36). In this context, Jianxin et al. (Ref 17) have previously suggested that Y_2O_3 doping influenced the mass transport of the Al_2O_3 matrix grains by controlling the diffusion of Al and O ions and improved the thermal stability of Al_2O_3, thus led nanocomposites to higher densities.

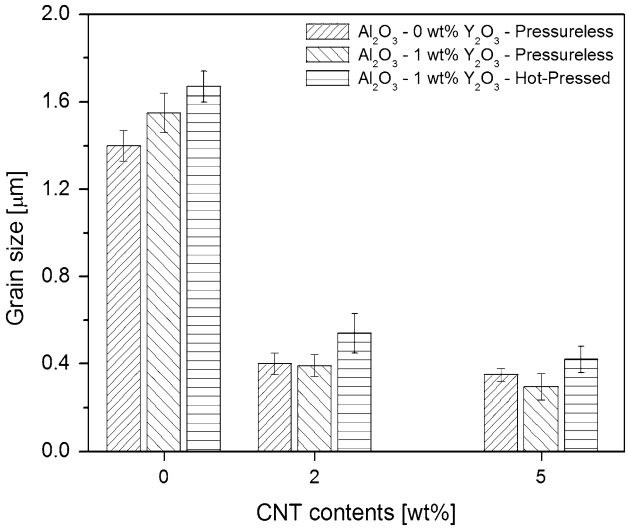

Fig. 6 Effect of CNTs concentrations, Y_2O_3 doping and sintering conditions on the grain size of Al_2O_3

Low magnification topographic details, as shown in Fig. 8, of the fractured surfaces of the monolithic Al_2O_3 and the CNT-reinforced nanocomposites sintered by pressureless and pressure-assisted methods revealed the densification problems associated with nanocomposites. Pressureless sintered

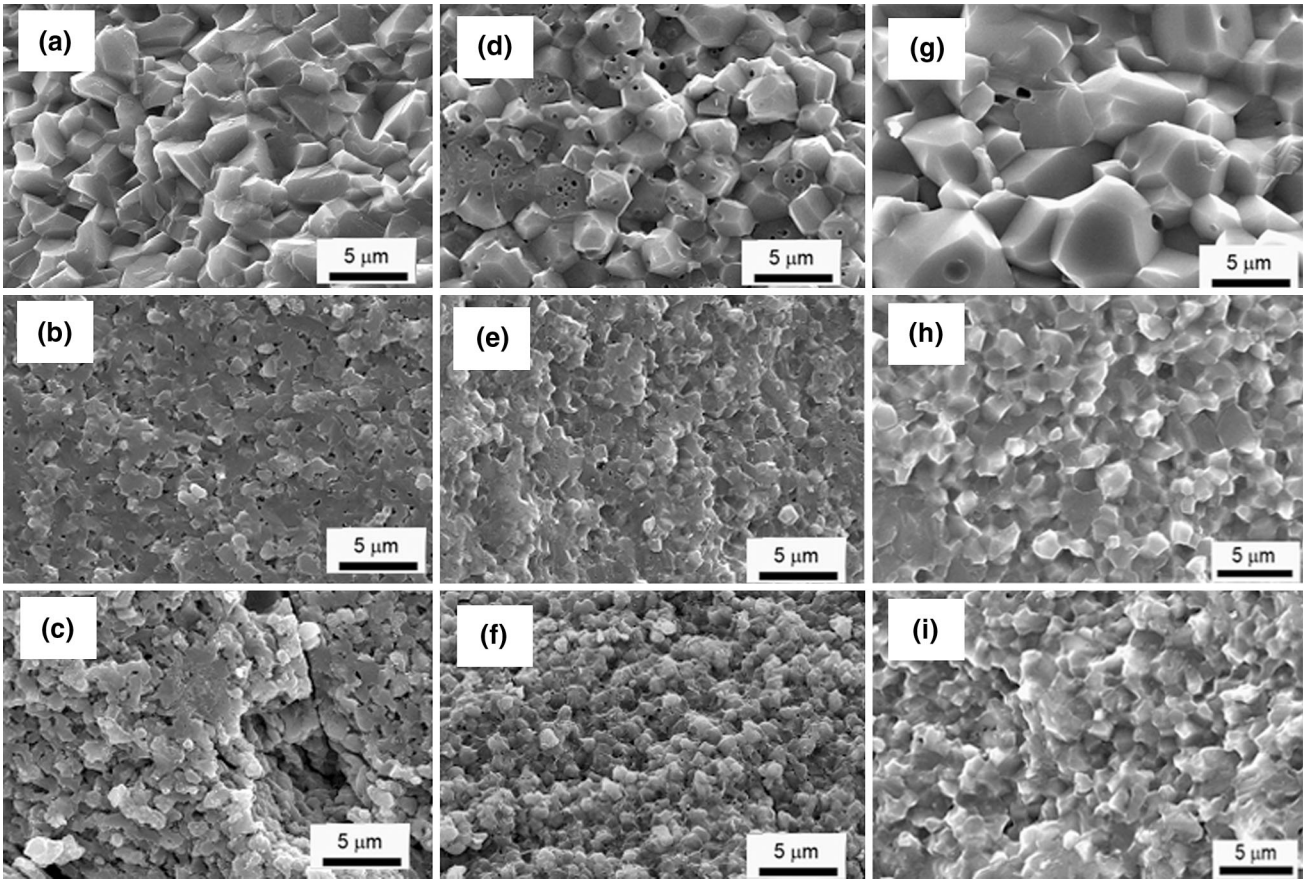

Fig. 7 SEM images of fractured surface of pressureless sintered (a) undoped Al_2O_3, (b) Al_2O_3-2 wt.% CNT, (c) Al_2O_3-5 wt.% CNT, (d) Al_2O_3-1 wt.% Y_2O_3, (e) Al_2O_3-1 wt.% Y_2O_3-2 wt.% CNT, (f) Al_2O_3-1 wt.% Y_2O_3-5 wt.% CNT and hot-pressed (g) Al_2O_3, (h) Al_2O_3-2 wt.% CNT and (i) Al_2O_3-5 wt.% CNT nanocomposite

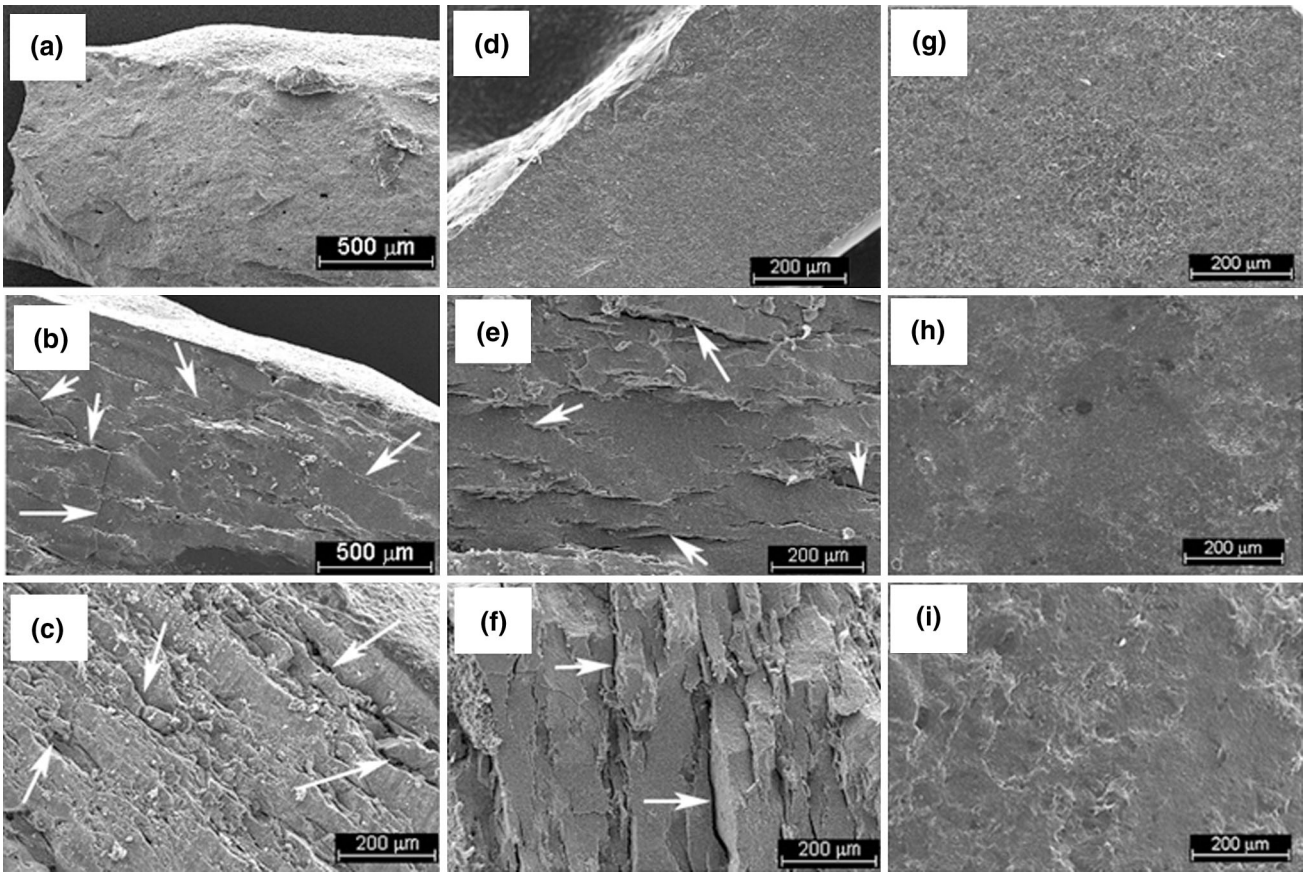

Fig. 8 Low magnification SEM images of the fractured surfaces of pressureless sintered (a) monolithic Al_2O_3, (b) Al_2O_3-2 wt.% CNT, (c) Al_2O_3-5 wt.% CNT, (d) Al_2O_3-1 wt.% Y_2O_3, (e) Al_2O_3-1 wt.% Y_2O_3-2 wt.% CNT and (f) Al_2O_3-1 wt.% Y_2O_3-5 wt.% CNT and hot-pressed (g) Al_2O_3-1 wt.% Y_2O_3, (h) Al_2O_3-1 wt.% Y_2O_3-2 wt.% CNT and (i) Al_2O_3-1 wt.% Y_2O_3-5 wt.% CNT

monolithic Al_2O_3 can be consolidated to higher densities to some extent and generates a homogenous microstructure, as shown in Fig. 8a. However, the addition of CNTs (2 wt.%) obviously worsened the densification process and produced heterogeneous structure as revealed in Fig. 8b. When adding 5 wt.% of CNTs, the densities and microstructure became even worse as shown in Fig. 8c.

Adding a small amount (1 wt.%) of Y_2O_3 sintering additives to plain Al_2O_3 facilitated the densification process in pressureless sintering, and slight improvement in microstructure was observed when compared with the undoped Al_2O_3 processed under identical conditions, Fig. 8(a) and (d). Similarly, CNT additions adversely influenced the densification process, leading to isolated dense patches separated by microcracks in the nanocomposites, as shown in Fig. 8(e) and (f). Thus, it can be concluded that CNTs are the main cause for the poor densification of the nanocomposites. During pressureless sintering, Al_2O_3 grains growth is restricted by CNTs accumulating at grain boundaries which lead to nanocomposites with fine grain structure by a pinning phenomenon. Meanwhile, this severely hampered the densification process, resulting in nanocomposites with porous or less dense structures. In this context, it has been found that at high temperature sintering at ~1600 °C, Al_2O_3 underwent a carbothermal reduction in the presence of CNTs which produced significant amounts of gaseous products such as Al_2O and CO, as reported (Ref 7, 35). In such cases, gases pressures inside the nanocomposite structures could be built up gradually, leading to microcracks, while escaping these gases during subsequent cooling process. Furthermore, the high aspect ratios of CNT also inhibited the densification of nanocomposites via interfering with the Al_2O_3 nanoparticles arrangement and with the shrinkage formation. This interference became stronger at higher CNT contents, and consequently inadequate densification with numerous microcracks was resulted, as marked by white arrows in Fig. 8 (Ref 37, 38).

In contrast to pressureless sintering, the presence of constant external pressures during HP constantly eliminated the nanocomposite from the formation of such microcracks and consolidated it effectively to higher densities by prevailing over the hurdles arising from CNTs. Therefore, HP had successfully integrated the grains of both monolithic Al_2O_3 and CNT-reinforced Al_2O_3 and produced a highly dense structure without the formation of any dense patches and microcracks, as shown in Fig. 8(g-i). It can be thus concluded that the presence of external pressure during high temperature sintering is essential for the consolidation of Al_2O_3-CNT nanocomposites, in order to achieve advanced structures and properties. It is also expected that Al_2O_3-CNT nanocomposites with high CNT volume fractions can be fabricated. Moreover, high-magnification SEM topographic details of the hot-pressed nanocomposite fractured surface, Fig. 9a, clearly demonstrate the fibrous morphology of the CNT and TEM study further confirms its tubular structure, as shown in Fig. 9b. It means that CNT has maintained its morphological characteristics, tubular structure, and nanoscale features even under severe sintering

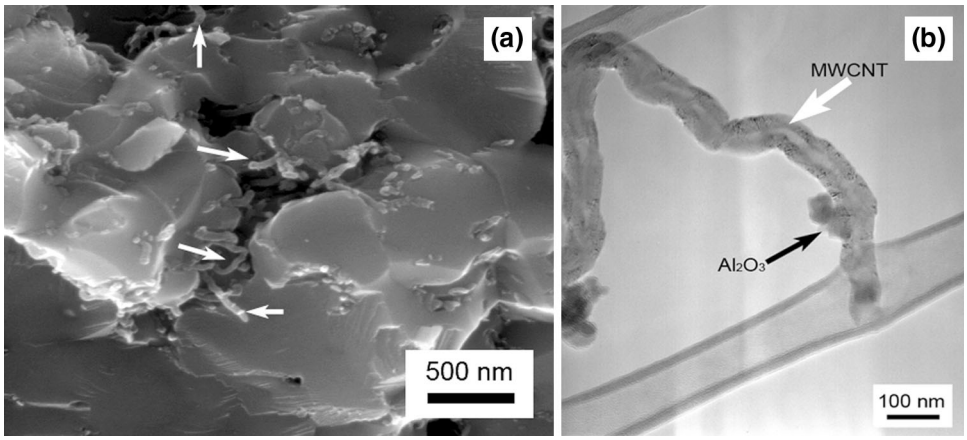

Fig. 9 (a) SEM images of fractured Al_2O_3-CNTs nanocomposites clearly showing the CNTs into Al_2O_3 matrix, (b) TEM image of the CNTs (white arrows) recovered from hot-pressed nanocomposites

Table 1 Properties of hot-pressed Y_2O_3 doped Al_2O_3 nanocomposites

Matrix material	CNT contents, wt.%	Y_2O_3 contents, wt.%	Modulus of elasticity, E GPa	Flexural strength, σy, MPa	Fracture toughness, K_{IC}, MPa $m^{1/2}$
Al_2O_3	0	1	392 ± 10	340 ± 32	3.1 ± 0.1
Al_2O_3	2	1	374 ± 16	380 ± 12	4.2 ± 0.3
Al_2O_3	5	1	291 ± 21	360 ± 10	3.5 ± 0.2

conditions of elevated temperatures and high pressures. High thermal stability of the CNT has been predicted in several molecular dynamics simulation studies and obtained features by electron microscope investigation in this study support these postulations (Ref. 39).

3.4 Mechanical Properties

The actual effect of uniform CNTs dispersion within the matrix was evaluated by measuring the microhardness. The measurement has shown that good CNT dispersions led Al_2O_3-CNT nanocomposites to higher hardness, while agglomeration resulted in lower microhardness and the results are graphically summarized in Fig. 4a. Figure 4d shows that low CNT contents (<1 wt.%) doped with Y_2O_3 resulted in increased microhardness but at higher CNT concentrations, no significant effect was observed. 10, 12, 11, 4, and 2% higher microhardness for nanocomposites containing 0, 0.5, 1.0, 2.0, and 5.0 wt.% of CNTs, respectively, have been obtained for Al_2O_3 containing 1 wt.% Y_2O_3, in comparison with undoped samples. Figure 4a clearly illustrates the constructive effects of CNT dispersions on the properties of Al_2O_3-CNT nanocomposites, and the well-dispersed CNTs led to nanocomposites with higher hardness. On the contrary, when bundles/lumps of CNT occurred, there was no interaction between the CNTs within the bundle and the matrix, and the lumps acted as an impurity and/or cavity, without any reinforcing effect, resulting in mechanically weakened nanocomposites (Ref 28, 40). However, as the second phase, even for well-dispersed CNTs, they have adverse effects on two important sintering parameters, the porosity elimination and the material diffusion (Ref 41). Constant pressure during the HP consolidated the Al_2O_3-CNT nanocomposites led to higher densities and promising improvement of 19 and 70% in microhardness at 2 and 5 wt.% CNTs loading, respectively, compared to the same samples consolidated by pressureless sintering, as shown in Fig. 4d. These results support that the pressure applied during the high temperature sintering is imperative to manufacture CNT-reinforced Al_2O_3 owing to high mechanical properties. Indeed, external pressure improved the densities by eliminating the structural defects and simultaneously Y_2O_3 controlled the sintering mechanisms (mass transportation and pore mobility), and thus led nanocomposite to improved hardness. Compared to doped monolithic Al_2O_3, a moderate rise in fracture toughness (10 and 5%) and flexural strength (26 and 11%) for the nanocomposites reinforced with 2 and 5 wt.%, respectively, was observed, as shown in Table 1. The improved fracture toughness and flexural strength are probably due to an enhanced load sharing by the well-dispersed CNTs which also confirmed the good adhesion between CNT and the matrix, as suggested in previous studies (Ref 7, 35). Furthermore, well-dispersed CNTs form individual interactions with the Al_2O_3 nanoparticles and can act as reinforcements which form bridges between cracked surfaces. Thus, the higher microhardness, fractured toughness, and strength of Y_2O_3-doped nanocomposites may be associated with the obtained higher densities, grain refinement by CNTs, and CNT's crack bridging/pull-out toughening mechanism, as suggested in several reports (Ref 2-13).

4. Conclusions

Homogenous dispersion of CNTs into the parent Al_2O_3 matrix was attained by opting relatively simple colloidal chemistry route after tweaking the key processing variables such as ultrasonication time, surfactant (SDS) contents, and CNTs/aqueous suspensions incubation durations. Y_2O_3

contents were optimized for the better densification of CNTs-reinforced Al_2O_3 and merely 1 wt.% Y_2O_3 additions densified pressureless sintered monolithic Al_2O_3 and its nanocomposites at low CNT concentrations (<1 wt.%) to higher densities; however, they barely influence at higher CNT contents. Nominal increase in densities (5, 6, 8, 7, and 6%) and hardness (10, 12, 11, 4, and 2%) as a function of CNT additions (0, 0.5, 1.0, 2.0, and 5.0 wt.%) was observed in 1 wt.% Y_2O_3-doped nanocomposites after sintering without pressure. Heterogeneous microstructures with isolated dense patches separated by microcracks elucidated the meager densities and mechanical performance of pressureless sintered nanocomposites. Simultaneous action of pressure and elevated temperatures during HP led 1 wt.% Y_2O_3-doped nanocomposites to fairly homogenous microstructures without evident structural irregularities. Indeed, Y_2O_3 contributed in improving densification process by controlling the material diffusion mechanism and by segregating at grain boundaries/triple-grain junctions as another $Y_3Al_5O_{12}$ phase. As a result, improved densities (7 and 15%) and hardness (11, and 12%) of hot-pressed Y_2O_3-doped Al_2O_3 samples reinforced with higher CNT contents (2 and 5 wt.%), respectively, were obtained compared to similar but pressureless sintered samples. Moreover, Y_2O_3-doped Al_2O_3 demonstrated propitious improvements in key mechanical properties like hardness (19, 70%), fracture toughness (10, 5%), and flexural strength (26, 11%) for higher (2, 5 wt.%) CNTs loadings, respectively, than doped but CNT-free Al_2O_3. Based on these results, it may be postulated that superior quality Al_2O_3-CNT nanocomposites, even at higher CNT loadings (>2 wt.%), can be prepared by using the combination of small amounts ($\sim$1 wt.%) of Y_2O_3, as dopant, and continuous high pressures during sintering process.

Acknowledgments

IA appreciates the financial support from the Center of Excellence for Research in Engineering Materials (CEREM), Advanced Manufacturing Institute (AMI), King Saud University (KSU), and Kingdom of Saudi Arabia. Authors are grateful to all the technical staff of CEREM laboratories for their kind assistance in material characterization. The first author is very thankful to Prof. Yanqiu Zhu of Exeter University, United Kingdom for his kind contribution in this study.

References

1. E.T. Thostenson, Z. Ren, and T.W. Chao, Advances in the Science and Technology of Carbon Nanotubes and their Composites: A Review, *Compos. Sci. Technol.*, 2001, **16**, p 1899–1912
2. A. Peigney, C. Laurent, and A. Rousset, Carbon Nanotube Novel Ceramic Matrix Nanocomposites, *Ceram. Int.*, 2000, **26**, p 677–683
3. L. Osayande and I. Okoli, Fracture Toughness Enhancement for Alumina System: A Review, *Int. J. Appl. Ceram. Technol.*, 2008, **5**, p 313–323
4. N.P. Padture, Multifunctional Composites of Ceramics and Single-Walled Carbon Nanotubes, *Adv. Mater.*, 2009, **21**, p 1767–1770
5. J. Fan, D. Zhao, and J. Song, Preparation and Microstructure of Multi-Walled Carbon Nanotubes Toughened Al_2O_3 Composite, *J. Am. Ceram. Soc.*, 2006, **89**, p 750–753
6. G. Zhan, J. Kuntz, J. Wan, and K. Mukherjee, Single-Walled Carbon Nanotubes as Attractive Toughing Agent in Alumina Based Nanocomposites, *Nat. Mater.*, 2003, **2**, p 38–42
7. I. Ahmad, A. Kennedy, and Y.Q. Zhu, Multi-Walled Carbon Nanotubes Reinforced Al_2O_3 Nanocomposites: Mechanical Properties and Interfacial Investigations, *Compos. Sci. Technol.*, 2010, **70**, p 1199–1206
8. F. Inam, T. Pijis, and M.J. Reece, The Production of Advanced Fine-Grained Alumina by Carbon Nanotubes Addition, *J. Eur. Ceram. Soc.*, 2011, **31**, p 2853–2859
9. I. Ahmad, H. Cao, H. Chen, H. Zhao, A. Kennedy, and Y.Q. Zhu, Carbon Nanotube Toughened Aluminium Oxide Nanocomposites, *J. Eur. Ceram. Soc.*, 2009, **30**, p 865–873
10. F. Inam and M.J. Reece, Electrically Conductive Alumina-Carbon Nanotubes Prepared by Spark Plasma Sintering, *J. Eur. Ceram. Soc.*, 2010, **30**, p 153–157
11. J. Sun and L. Gao, Development of a Dispersion Process for Carbon Nanotubes in Ceramic Matrix by Hetero-Coagulation, *Carbon*, 2003, **41**, p 1063–1068
12. B. Chan and I. Seung, Fabrication of CNT-Reinforced Al_2O_3 Matrix Nanocomposites by Sol-Gel, *Mater. Sci. Eng.*, 2005, **395**, p 124–128
13. C.S. Zhang, W.G. Fahrenholtz, G.E. Hilmas, and J.Y. Edward, Pressureless Sintering of Carbon Nanotube—Al_2O_3 Composites, *J. Eur. Ceram. Soc.*, 2010, **30**(6), p 1373–1380
14. J. Wang, S.Y. Lim, and C.H. Chew, Dramatic Effect of a Small Amount of MgO Addition on the Sintering of Al_2O_3—5 vol.% SiC Nanocomposite, *Mater. Lett.*, 1998, **33**, p 273–277
15. Y.K. Jeong, A. Nakahira, and K. Niihara, Effects of Additives on Microstructure and Properties of Al_2O_3—Silicon Carbide Nanocomposites, *J. Am. Ceram. Soc.*, 1999, **82**, p 3609–3612
16. D.A. Rani, Y. Yoshizawa, K. Hirao, and Y. Yamushi, Effect of Rare-Earth Dopants on Mechanical Properties of Al_2O_3, *J. Am. Ceram. Soc.*, 2008, **87**, p 289–292
17. F. Jianxin, A.M. Thompson, M.P. Harmer, and H.M. Chan, Effect of Yttrium and Lanthanum on the Final-Stage Sintering Behavior of Ultrahigh-Purity Al_2O_3, *J. Am. Ceram. Soc.*, 1997, **80**, p 2005–2012
18. S. Lartigue, C. Carry, and L. Priester, Grain Boundaries in High Temperature Deformation of Yttria and Magnesia Co-Doped Alumina, *J. Phys. Colloq.*, 1990, **51**, p 985–990
19. D. Delaunay, A.M. Huntz, and P. Lacombe, The Influence of Yttrium on the Sintering of Al_2O_3, *J. Less Common Met.*, 1980, **70**, p 115–117
20. Y.K. Jeong, A. Nakharia, and K. Niihara, Effect of Additives on Microstructure and Properties of Al_2O_3 Silicon Carbide Nanocomposite, *J. Am. Ceram. Soc.*, 1999, **82**, p 3069–3612
21. S.K.C. Pillai and S. Hamsphire, Controlling the Grain Growth in Yttria Doped Al_2O_3—5 wt.% SiC Nanocomposite Prepared by Pressureless Sintering, *J. Am. Ceram. Soc.*, 2004, **24**, p 3317–3326
22. A.G. Robertson, D.S. Wilkinson, and C.H. Caceres, Creep and Creep Fracture in Hot-Pressed Al_2O_3, *J. Am. Ceram. Soc.*, 1991, **74**, p 915–921
23. S. Lartigue and F. Dupau, Grain Boundary Behavior in Superplastic Mg-Doped Al_2O_3 with Yttria Co-doping, *Acta. Metal. Mater.*, 1994, **42**, p 293–302
24. F. Cesari, L. Esposito, F.M. Furgiuele, C. Maletta, and A. Tucci, Fracture Toughness of Al_2O_3-zirconia composites, *Ceram. Int.*, 2006, **32**, p 249–255
25. M. Ajayan, Nanotubes from Carbon, *Chem. Rev.*, 1999, **99**, p 1787–1799
26. T.K. Shen and P. Hing, Ultrasonic Through-Transmission Method of Evaluating the Modulus of Elasticity of Al_2O_3-ZrO_2 Composite, *J. Mater. Sci.*, 1997, **32**, p 6633–6638
27. G.R. Anstis, P. Chantikul, and D.B. Marshall, A Critical Evaluation of Indentation Technique for Measuring Fracture Toughness: I, Direct Crack Method, *J. Am. Ceram. Soc.*, 1986, **4**(1), p 533–538
28. J. Sun and L. Gao, Reinforcement of Al_2O_3 Matrix with Multi-Walled CNTs, *Ceram. Int.*, 2005, **31**, p 893–896
29. C.E. Borsa, H.S. Ferreira, and R.A. Kiminami, Liquid Phase Sintering of Al_2O_3/SiC, *J. Eur. Ceram. Soc.*, 1999, **19**, p 615–621
30. M. Alex, I. Todd, and S.G. Robert, Effects of Yttrium on the Sintering and Microstructure of Al_2O_3 Silicon Carbide Nanocomposites, *J. Am. Ceram. Soc.*, 2005, **88**(9), p 2354–2361
31. C.P.S. Kumar, B. Baron, and S. Hampshire, Effect of Dopants on Densification, Microstructure and Mechanical Properties of Al_2O_3-Silicon Nanocomposites Ceramics Prepared by Pressureless Sintering, *J. Eur. Ceram. Soc.*, 2004, **24**, p 3317–3326
32. J.D. Cawley and J.W. Halloran, Dopant Distribution in Nominally Yttrium-Doped Sapphire, *J. Am. Ceram. Soc.*, 1986, **69**, p 195–196
33. F. Danan, L.Q. Chen, and S.P. Chen, Numerical Simulation of Zener Pinning with Growing Second-Phase Particles, *J. Am. Ceram. Soc.*, 1998, **81**, p 526–532

34. R.L. Coble, Diffusion Models for Hot Pressing with Surface Energy and Pressure Effects as Driving Forces, *J. Appl. Phys.*, 1970, **41**, p 4798–4808
35. S. Sarkar and P.K. Das, Microstructure and Physicomechanical Properties of Pressure-Less Sintered Multi-Walled Carbon Nanotube/Alumina Nanocomposites, *Ceram. Int.*, 2012, **38**, p 423–432
36. O. Thomas and J. Rodel, Evolution of Mechanical Properties of Porous Al_2O_3 During Free Sintering and Hot Pressing, *J. Am. Ceram. Soc.*, 1999, **82**, p 3080–3086
37. M.S. Lee, *Handbook of Composites Reinforcements*, Wiley-Blackwell, New York, 1992, p 151
38. M. Chen, F.R. Jones, and J.E. Bailey, The Role of Interface on the Densification of Sol-Gel Processed Al_2O_3 and Mullite Fibre Composites, *Inst. Phys. Conf. Ser.*, 1990, **111**, p 227–237
39. K.M. Liew, C.H. Wong, X.Q. He, and M.J. Tan, Thermal Stability of Single and Multi-Walled Carbon Nanotubes, *Phys. Rev.*, 2005, **B71**, p 075424
40. Z. Xia, W.A. Curtain, and B.W. Sheldon, Fracture Toughness of Highly Ordered Carbon Nanotubes/Al_2O_3 Nanocomposite, *Trans. ASME*, 2004, **126**, p 224–238
41. C. Laurent, A. Peigney, and A. Rousset, Carbon Nanotubes-Fe-Al_2O_3 Nanocomposites. Part II: Microstructure and Mechanical Properties of the Hot-Pressed Composites, *J. Eur. Ceram. Soc.*, 1998, **18**, p 2005–2013